Bending analysis of functionally graded nanoplates based on a higher-order shear deformation theory using dynamic relaxation method

M. E. Golmakani[1], Mohammad Malikan[2]*, S. Golshani Pour[1], Victor A. Eremeyev[2,3,4]

[1] Department of Mechanical Engineering, Mashhad Branch, Islamic Azad University, Mashhad, Iran;
[2] Department of Mechanics of Materials and Structures, Faculty of Civil and Environmental Engineering, Gdansk University of Technology, 80-233 Gdansk, Poland;
[3] Research and Education Center "Materials" Don State Technical University, Gagarina sq., 1, 344000 Rostov on Don, Russia
[4] Department of Civil and Environmental Engineering and Architecture (DICAAR), University of Cagliari, Via Marengo, 2, Cagliari 09123, Italy
* Correspondence: mohammad.malikan@pg.edu.pl, mohammad.malikan@yahoo.com

Abstract: In this paper, bending analysis of rectangular functionally graded (FG) nanoplates under a uniform transverse load has been considered based on the modified couple stress theory. Using Hamilton's principle, governing equations are derived based on a higher-order shear deformation theory (HSDT). The set of coupled equations are solved using the dynamic relaxation (DR) method combined with finite difference (FD) discretization technique for clamped and simply-supported boundary conditions. Finally, the effects of aspect ratio, thickness-to-length ratio, transverse load, boundary conditions, and length scale parameter are studied in detail. The results showed that by rising the length scale-to-thickness ratio, the influence of the grading index on the deflection decreased.

Keywords: Bending analysis; FG nanoplates; Modified couple stress theory; HSDT; DR

1. Introduction

Owing to the magnificent mechanical, electrical, chemical, and thermal properties of the nanostructures, they have obtained the attention of many researchers. One of the typical structures of nano-systems is two-dimensional nanoplates with superior mechanical characteristics compared to conventional engineering materials. Because of the unique properties of nanoplates, they have a wide range of potential applications in different industries, and several solution methods such as experimental, analytical, and numerical approaches are used to recognize the mechanical behavior of these kinds of materials. Recently, many experiments have shown that the mechanical behavior of materials in micro size and even smaller sizes are affected by the small dimensions [1, 2]. The size dependency property of materials is an intrinsic parameter that appeared whilst the characteristic length of the material (thickness, diameter, etc.) could be compared with the material length scale parameter [1, 3]. This length scale parameter is a mechanical property but not constant that has been determined like other mechanical properties of materials in an amplitude amount [1]. Classical continuum mechanics is not able to describe size dependency behavior. In order to correct this inability of classical continuum mechanics, the size-dependent continuum theories have been presented within which modified couple stress theory [4] and strain gradient theory [5] as the first

gradient model of Mindlin are interesting for the researchers owing to their simplicity and high accuracy results. In the case of second Mindlin's gradient model, there are interests among researchers as well [6-8]. It is worth noting that the size-dependent theories have further constants than classical ones in which only Lamé constants are used for isotropic materials. So that the modified couple stress, first strain gradient and second strain gradient theories have 1 to three further constants more rather than Lamé constants for isotropic materials [4, 5, 9, 10]. Up to now, the size-dependent mechanical behavior of micro and nanobeams has been investigated by many researchers using the modified couple stress theory. But, the mechanical behavior of micro and nanoplates are limited in number based on this theory. Tsiatas [11] investigated the size-dependent mechanical behavior of thin plates with arbitrary shapes using the Kirchhoff assumption. He showed that considering small size effects increases the rigidity of microplates. Asghari [12] presented a size-dependent model for nonlinear analysis of thin plates with arbitrary shapes based on the modified couple stress theory. Jomehzadeh et al. [13] examined the effect of size on the natural frequencies of rectangular and circular thin microplates with the modified couple stress theory in conjunction with the classical plate hypothesis. They noticed that considering size effects leads to increasing natural frequencies of the system. Akgöz and Civalek [14] investigated bending, buckling, and free vibrations of rectangular microplates embedded on an elastic foundation using analytical solutions for simply-supported boundary conditions. Ke et al. [15] utilized the modified couple stress theory for calculating natural frequencies of thick plates based on first-order shear deformation theory (FSDT). They solved the governing equations with the P-type Ritz method and found that the influence of size was drastically increased whilst the thickness of the plate is equal with its material length scale parameter. Roque et al. [16] also studied static bending of thick microplates using the modified couple stress theory in conjunction with Mindlin plate theory. A finite element size-dependent model has been presented by Zhang et al. [17] for static bending, buckling, and free vibration of thick microplates by considering modified couple stress theory and Mindlin assumptions. The presented rectangular element was covered by 4 nodes and 15 degrees of freedom at every node. Using the differential quadrature method (DQM), Ke et al. [18] considered static bending, buckling, and free vibration of thick annular microplates made of functionally graded materials (FGMs) by using modified couple stress theory and Mindlin assumptions. Thai and Choi [19] presented size-dependent nonlinear and linear models for static bending, buckling and free vibrations of rectangular microplates made of functionally graded materials based on Kirchhoff and Mindlin's hypothesizes by using modified couple stress theory. They considered this model for plates with simply-supported boundary conditions. Similar research also was carried out by Thai and Kim [20] with the difference that the Reddy hypothesis was used. Malikan considered biaxial buckling of nanoplates [21, 22] and shear buckling of piezoelectric nanoplates [23, 24] using modified couple stress theory. The results showed that the length scale parameter in couple stress models led to increasing stiffness of the nanoplates in various boundary conditions. Abo-bakr et al. [25] investigated a macro beam with FGM properties subject to an axial loading. The analysis included optimization of the weight of the material based on the Pareto optimality. A higher-order shear deformation beam hypothesis provided the equilibrium equations to solution of which the DQM was employed. Abdelrahman et al. [26] performed a study on the static deflections of a perforated microscale beam containing microscale influences using a couple stress model. The study also incorporated both Euler-Bernoulli and Timoshenko approaches. Another research done by Esen et al. [27] on the dynamics of small scale structures to which couple stress theory was used. Abo-Bakr et al. [28] analyzed a FG nanobeam involving electro-mechanical effects under pull-in instability. Different approaches were applied to capture small scale influences, such as Gurtin–Murdoch surface elasticity and the modified couple stress theory.

Further literature in the field of the current topic is available which due to the sake of brevity can be seen as [29-37].

In this research, based on modified couple stress theory bending of a rectangular functionally graded nanoplate is investigated using dynamic relaxation method (DRM). The equations are derived based on a higher-order shear deformation plate theory. The set of coupled equations are solved for clamped and simply-supported boundary conditions. Finally, the effects of aspect ratio,

thickness-to-length ratio, transverse load, boundary conditions, and length scale parameter are studied in detail.

2. Formulation

The nanoplate is considered with length L_x, width L_y, and thickness h as shown in Fig. 1 in the Cartesian coordinate system. The plate is subjected to the transverse static load (q_x) and rested on the elastic foundation.

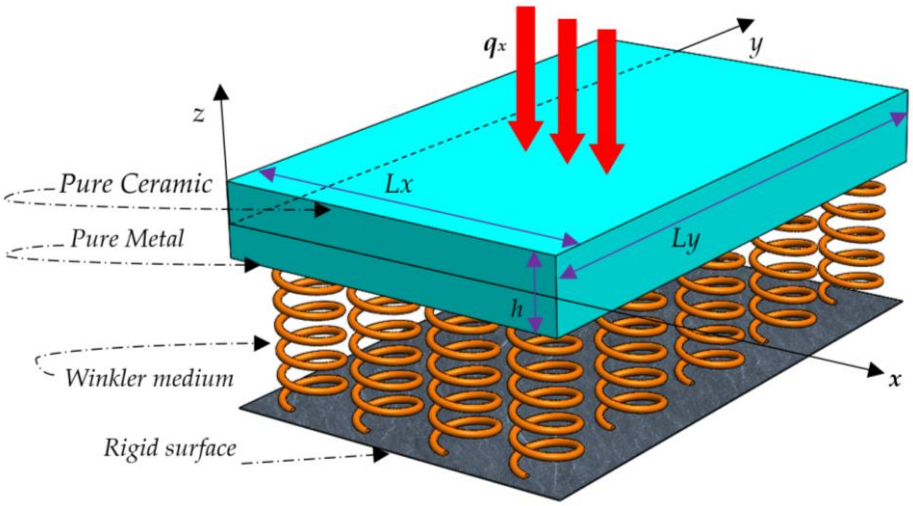

Figure 1. Schematic diagram of a rectangular FG nanosheet under uniform transverse load.

The displacement field of higher-order shear deformation plate theory is defined as follows:

$$\begin{aligned} u(x,y,z) &= u_0(x,y) - z\frac{\partial w_0}{\partial x} + f(z)\varphi_x(x,y) \ , \\ v(x,y,z) &= v_0(x,y) - z\frac{\partial w_0}{\partial y} + f(z)\varphi_y(x,y) \ , \\ w(x,y,z) &= w_0(x,y) \end{aligned} \tag{1}$$

in which

$$\begin{aligned} f(z) &= h\tan^{-1}\left(\frac{2}{h}z\right) - z \ , \\ g(z) &= f'(z) = \frac{(1-(\frac{2}{h}z)^2)}{(1+(\frac{2}{h}z)^2)} \ , \\ k(z) &= f''(z) = \frac{-\frac{16}{h^2}z}{(1+(\frac{2}{h}z)^2)^2} \end{aligned} \tag{2}$$

In light of the strain-displacement relations in Lagrangian form:

$$\varepsilon_{ij} = \frac{1}{2}\left[\frac{\partial u_i}{\partial x_j} + \frac{\partial u_j}{\partial x_i}\right] \tag{3}$$

By substituting Eq. (1) into Eq. (3) the strain field based on the displacements are as follows:

$$\begin{aligned} \varepsilon_{xx} &= \frac{\partial u_0}{\partial x} - z\frac{\partial^2 w_0}{\partial x^2} + f(z)\frac{\partial \varphi_x}{\partial x}, \\ \varepsilon_{yy} &= \frac{\partial v_0}{\partial y} - z\frac{\partial^2 w_0}{\partial y^2} + f(z)\frac{\partial \varphi_y}{\partial y}, \end{aligned} \tag{4}$$

$$\varepsilon_{zz} = 0,$$

$$\gamma_{xy} = \frac{\partial u_0}{\partial y} + \frac{\partial v_0}{\partial x} - 2z\frac{\partial^2 w_0}{\partial x \partial y} + f(z)\left(\frac{\partial \varphi_x}{\partial y} + \frac{\partial \varphi_y}{\partial x}\right),$$

$$\gamma_{xz} = g(z)\varphi_x,$$

$$\gamma_{yz} = g(z)\varphi_y$$

Different methods consider the issue of achieving suitable functions for modeling the material properties of FGMs. In this study, the simple rule of the mixture has been employed to express the elasticity modulus of the functionally graded material which is made by ceramics and metals as follows:

$$E(z) = E_m + (E_c - E_m)\, V(z) \ , \tag{5}$$

where $V(z)$ is the volume fraction which is defined by [38-47]

$$V(z) = (\frac{1}{2} + \frac{z}{h})^n, \tag{6}$$

In Eqs. (5) and (6), E_m is Young's modulus of metals, E_c denotes Young's modulus of ceramics and n represents the grading index for the material. It is to be noted that the Poisson's ratio is supposed to be constant as ν. The small scale effect has been considered by the modified couple stress theory, which was developed by Yang et al. [48]. In this theory, strain energy is a function of both strain tensor (the strain related to strain tensor) and curvature (relevant to couple stress tensor). In fact, they defined strain energy as the following Hamiltonian formulas:

$$U = \frac{1}{2}\int\left(\sigma_{ij}\varepsilon_{ij} + m_{ij}\chi_{ij}\right)d\,V, \tag{7}$$

where ε is the strain tensor, σ is the stress tensor, χ is the curvature symmetrical tensor and m is the lateral section of couple stress tensor which are obtained in the following equations [21-24, 49]:

$$\chi_{ij} = \frac{1}{2}\left(\frac{\partial \theta_i}{\partial x_j} + \frac{\partial \theta_j}{\partial x_i}\right),$$

$$\theta_i = \frac{1}{2}(curl(u))_i, \tag{8}$$

$$m_{ij} = 2l^2\mu\chi_{ij}$$

Upon physical view, large interactions between lattice's atoms and large strain gradient of atoms oblige the theoretical studies on nanoscale to a different constitutive formulation based on size-dependent continuum models. Mathematically, these models are up to differential or integral forms. From a macro scale point of view, interactions in a plane of material are short and mostly between neighbor crystalline. Hence, strain non-localization implemented by couple stress theories can help us to study large strain gradient of atoms. High contrast composite nanostructures such as FGMs may be worthy of investigation in the case of size-dependency. Strain gradient phenomena occurs in beam-lattice structures with homogeneity. The nano-beam/plate continua include large strain gradient resists against mechanical deformations and intrinsic reaction of the structure will change due to the strain gradient. Generally, modelling the nanoscale on the basis of the strain gradient leads to accuracy in forecasting of mechanical deformation of micro/nanostructures.

With respect to Eq. (8), the length scale parameter (l) is the square of curvature module to shear module ratio, mathematically, and as a physical definition indicates the effect of the coupled stress. A sub-micro scale structure reacts entirely dissimilar with local structures which are usually at macro scale. These different response leads to being the material size-dependent. Therefore, this kind of material requires exclusive modelling to be investigated mechanically. With respect to the current size-dependent theoretical models, we are confronting with additional small scale parameters that are sometimes called as length scale parameters. There is one small scale factor in the couple stress

theory that the values of it cannot be constant [50]. However, the values of this length scale parameter are not provided for many materials yet. From physical point of view, it relates to the internal property as well as external conditions of the structure. The value will differ by a change in the boundary conditions. High costs of experimental analysis tend us to employ these vital parameters. Exerting these scaled-values parameters results in anticipation of strength of scaled-down structures. Some researchers already found some values for the length scale factor [51-54]. Normally, experiments are necessity to identify values of these size parameter. However, the obtained values will be in arrange for a material under a special analysis depending on the physical conditions of the specimen. To this end, the values of laboratory works should be adopted with the values of theoretical model by choosing an amplitude for the values. After that it can be found that the values of the parameter are existed between two certain digits. Until now, no body has presented that this value can be a material constant resemblance to Lame' constants. Instead, the reasonable limit for the value of this parameter could be the best choice.

According to the displacement field and Eq. (8), the following relations are expressed:

$$\begin{aligned}
\theta_1 &= \frac{\partial w_0}{\partial y} - \frac{g(z)}{2}\varphi_y, \\
\theta_2 &= -\frac{\partial w_0}{\partial x} + \frac{g(z)}{2}\varphi_x, \\
\theta_3 &= \frac{1}{2}\left(\frac{\partial v_0}{\partial x} - \frac{\partial u_0}{\partial y}\right) + \frac{f(z)}{2}\left(\frac{\partial \varphi_y}{\partial x} - \frac{\partial \varphi_x}{\partial y}\right), \\
\chi_{xx} &= \frac{\partial^2 w_0}{\partial x \partial y} - \frac{g(z)}{2}\frac{\partial \varphi_y}{\partial x}, \\
\chi_{yy} &= -\frac{\partial^2 w_0}{\partial x \partial y} + \frac{g(z)}{2}\frac{\partial \varphi_x}{\partial y}, \\
\chi_{zz} &= \frac{g(z)}{2}\left(\frac{\partial \varphi_y}{\partial x} - \frac{\partial \varphi_x}{\partial y}\right), \\
\chi_{xy} &= \frac{1}{2}\left(\frac{\partial^2 w_0}{\partial y^2} - \frac{\partial^2 w_0}{\partial x^2}\right) + \frac{g(z)}{4}\left(\frac{\partial \varphi_x}{\partial x} - \frac{\partial \varphi_y}{\partial y}\right), \\
\chi_{xz} &= \frac{1}{4}\left[\left(\frac{\partial^2 v_0}{\partial x^2} - \frac{\partial^2 u_0}{\partial x \partial y}\right) + f(z)\left(\frac{\partial^2 \varphi_y}{\partial x^2} - \frac{\partial^2 \varphi_x}{\partial x \partial y}\right) - k(z)\varphi_y\right], \\
\chi_{yz} &= \frac{1}{4}\left[\left(\frac{\partial^2 v_0}{\partial x \partial y} - \frac{\partial^2 u_0}{\partial y^2}\right) + f(z)\left(\frac{\partial^2 \varphi_y}{\partial x \partial y} - \frac{\partial^2 \varphi_x}{\partial y^2}\right) + k(z)\varphi_x\right]
\end{aligned} \tag{9}$$

Furthermore, with regard to Eq. (7) the virtual strain energy relation can be expanded as:

$$\begin{aligned}
\delta U = \iint &\left(\sigma_{xx}\delta\varepsilon_{xx} + \sigma_{yy}\delta\varepsilon_{yy} + \sigma_{xy}\delta\gamma_{xy} + \sigma_{xz}\delta\gamma_{xz} + \sigma_{yz}\delta\gamma_{yz}\right)dAdz \\
&+ \left(m_{xx}\delta\chi_{xx} + m_{yy}\delta\chi_{yy} + m_{zz}\delta\chi_{zz} + 2m_{xy}\delta\chi_{xy} + 2m_{xz}\delta\chi_{xz} + 2m_{yz}\delta\chi_{yz}\right)dAdz
\end{aligned} \tag{10}$$

By using Eq. (10), the governing equations of the nanoplate are obtained:

$$\delta u=0:$$

$$\frac{\partial N_{xx}}{\partial x} + \frac{\partial N_{xy}}{\partial y} + \frac{1}{2}\left(\frac{\partial^2 R_{xz}}{\partial x \partial y} + \frac{\partial^2 R_{yz}}{\partial y^2}\right) = 0, \tag{11}$$

$$\delta v=0;$$

$$\frac{\partial N_{xy}}{\partial x}+\frac{\partial N_{yy}}{\partial y}-\frac{1}{2}\left(\frac{\partial^2 R_{xz}}{\partial x^2}+\frac{\partial^2 R_{yz}}{\partial x\partial y}\right)=0,$$

$\delta w_0=0$:

$$\frac{\partial^2 M_{xx}}{\partial x^2}+2\frac{\partial^2 M_{xy}}{\partial x\partial y}+\frac{\partial^2 M_{yy}}{\partial y^2}+\frac{\partial^2 R_{xy}}{\partial x^2}-\frac{\partial^2 R_{xy}}{\partial y^2}+\frac{\partial^2\left(R_{yy}-R_{xx}\right)}{\partial x\partial y}+q_{eff}=0,$$

$\delta\varphi_x=0$:

$$\frac{\partial P_{xx}}{\partial x}+\frac{\partial P_{xy}}{\partial y}-Q_{xz}+\frac{1}{2}\left(\frac{\partial S_{xy}}{\partial x}+\frac{\partial S_{yy}}{\partial y}-\frac{\partial S_{zz}}{\partial y}+\frac{\partial^2 T_{xz}}{\partial x\partial y}+\frac{\partial^2 T_{yz}}{\partial y^2}-L_{yz}\right)=0,$$

$\delta\varphi_y=0$:

$$\frac{\partial P_{xy}}{\partial x}+\frac{\partial P_{yy}}{\partial y}-Q_{yz}-\frac{1}{2}\left(\frac{\partial S_{xx}}{\partial x}+\frac{\partial S_{xy}}{\partial y}-\frac{\partial S_{zz}}{\partial x}+\frac{\partial^2 T_{xz}}{\partial x^2}+\frac{\partial^2 T_{yz}}{\partial x\partial y}+L_{xz}\right)=0,$$

In Eq. (11), the means of q_{eff} is external forces which are defined by [55, 56]:

$$q_{eff}=q-k_w w_0, \tag{12}$$

in which k_w and q represent the elastic matrix and the transverse uniform static load, respectively. Moreover, the stress and couple stress resultants are written as:

$$\begin{aligned}\left(N_{ij},M_{ij},P_{ij},Q_{ij}\right)&=\int_{-\frac{h}{2}}^{\frac{h}{2}}\left(1,z,f(z),g(z)\right)\sigma_{ij}dz,\\ \left(R_{ij},S_{ij},T_{ij},L_{ij}\right)&=\int_{-\frac{h}{2}}^{\frac{h}{2}}\left(1,g(z),f(z),k(z)\right)m_{ij}dz\end{aligned} \tag{13}$$

Eq. (13) can be expanded and splitted into some groups as follows:

1- Force and moment stress resultants:

$$\begin{aligned}N_{xx}&=A\left(\frac{\partial u_0}{\partial x}+\nu\frac{\partial v_0}{\partial y}\right)-B\left(\frac{\partial^2 w_0}{\partial x^2}+\nu\frac{\partial^2 w_0}{\partial y^2}\right)+C\left(\frac{\partial\varphi_x}{\partial x}+\nu\frac{\partial\varphi_y}{\partial y}\right),\\ N_{yy}&=A\left(\nu\frac{\partial u_0}{\partial x}+\frac{\partial v_0}{\partial y}\right)-B\left(\nu\frac{\partial^2 w_0}{\partial x^2}+\frac{\partial^2 w_0}{\partial y^2}\right)+C\left(\nu\frac{\partial\varphi_x}{\partial x}+\frac{\partial\varphi_y}{\partial y}\right),\\ N_{xy}&=A\frac{1-\nu}{2}\left(\frac{\partial u_0}{\partial y}+\frac{\partial v_0}{\partial x}\right)-B(1-\nu)\left(\frac{\partial^2 w_0}{\partial x\partial y}\right)+C\frac{1-\nu}{2}\left(\frac{\partial\varphi_x}{\partial y}+\frac{\partial\varphi_y}{\partial x}\right),\\ M_{xx}&=B\left(\frac{\partial u_0}{\partial x}+\nu\frac{\partial v_0}{\partial y}\right)-D\left(\frac{\partial^2 w_0}{\partial x^2}+\nu\frac{\partial^2 w_0}{\partial y^2}\right)+F\left(\frac{\partial\varphi_x}{\partial x}+\nu\frac{\partial\varphi_y}{\partial y}\right),\\ M_{yy}&=B\left(\nu\frac{\partial u_0}{\partial x}+\frac{\partial v_0}{\partial y}\right)-D\left(\nu\frac{\partial^2 w_0}{\partial x^2}+\frac{\partial^2 w_0}{\partial y^2}\right)+F\left(\nu\frac{\partial\varphi_x}{\partial x}+\frac{\partial\varphi_y}{\partial y}\right),\\ M_{xy}&=B\frac{1-\nu}{2}\left(\frac{\partial u_0}{\partial y}+\frac{\partial v_0}{\partial x}\right)-D(1-\nu)\left(\frac{\partial^2 w_0}{\partial x\partial y}\right)+F\frac{1-\nu}{2}\left(\frac{\partial\varphi_x}{\partial y}+\frac{\partial\varphi_y}{\partial x}\right),\\ Q_{xz}&=G(z)A\varphi_x,\\ Q_{yz}&=G(z)A\varphi_y,\end{aligned} \tag{14}$$

where $G(z)$ and A respectively denote the shear modulus of the FG materials and cross-section area.

2- Additional force and moment stress resultants originated from the higher-order beam theory:

$$P_{xx} = C\left(\frac{\partial u_0}{\partial x} + \nu\frac{\partial v_0}{\partial y}\right) - F\left(\frac{\partial^2 w_0}{\partial x^2} + \nu\frac{\partial^2 w_0}{\partial y^2}\right) + H\left(\frac{\partial \varphi_x}{\partial x} + \nu\frac{\partial \varphi_y}{\partial y}\right),$$

$$P_{yy} = C\left(\nu\frac{\partial u_0}{\partial x} + \frac{\partial v_0}{\partial y}\right) - F\left(\nu\frac{\partial^2 w_0}{\partial x^2} + \frac{\partial^2 w_0}{\partial y^2}\right) + H\left(\nu\frac{\partial \varphi_x}{\partial x} + \frac{\partial \varphi_y}{\partial y}\right),$$

$$P_{xy} = C\frac{1-\nu}{2}\left(\frac{\partial u_0}{\partial y} + \frac{\partial v_0}{\partial x}\right) - F(1-\nu)\left(\frac{\partial^2 w_0}{\partial x \partial y}\right) + H\frac{1-\nu}{2}\left(\frac{\partial \varphi_x}{\partial y} + \frac{\partial \varphi_y}{\partial x}\right),$$

3- Couple stress resultants:

$$R_{xx} = 2A_n\frac{\partial^2 w_0}{\partial x \partial y} - B_n\frac{\partial \varphi_y}{\partial x},$$

$$R_{yy} = -2A_n\frac{\partial^2 w_0}{\partial x \partial y} + B_n\frac{\partial \varphi_x}{\partial y},$$

$$R_{xy} = A_n\left(\frac{\partial^2 w_0}{\partial y^2} - \frac{\partial^2 w_0}{\partial x^2}\right) - \frac{B_n}{2\left(\frac{\partial \varphi_x}{\partial x} - \frac{\partial \varphi_y}{\partial y}\right)},$$

$$R_{xz} = \frac{A_n}{2}\left(\frac{\partial^2 v_0}{\partial x^2} - \frac{\partial^2 u_0}{\partial x \partial y}\right) + \frac{C_n}{2}\left(\frac{\partial^2 \varphi_y}{\partial x^2} - \frac{\partial^2 \varphi_x}{\partial x \partial y}\right) - \frac{K_{n1}}{2}\varphi_y,$$

$$R_{yz} = \frac{A_n}{2}\left(\frac{\partial^2 v_0}{\partial x \partial y} - \frac{\partial^2 u_0}{\partial y^2}\right) + \frac{C_n}{2}\left(\frac{\partial^2 \varphi_y}{\partial x \partial y} - \frac{\partial^2 \varphi_x}{\partial y^2}\right) + \frac{K_{n1}}{2}\varphi_x,$$

4- Additional couple stress resultants developed from the combination of the higher-order beam theory, FGM structure and the couple stress model:

$$S_{xx} = 2B_n\frac{\partial^2 w_0}{\partial x \partial y} - D_n\frac{\partial \varphi_y}{\partial x},$$

$$S_{yy} = -2B_n\frac{\partial^2 w_0}{\partial x \partial y} + D_n\frac{\partial \varphi_x}{\partial y},$$

$$S_{zz} = D_n\left(\frac{\partial \varphi_y}{\partial x} - \frac{\partial \varphi_x}{\partial y}\right),$$

$$S_{xy} = B_n\left(\frac{\partial^2 w_0}{\partial y^2} - \frac{\partial^2 w_0}{\partial x^2}\right) - \frac{D_n}{2\left(\frac{\partial \varphi_x}{\partial x} - \frac{\partial \varphi_y}{\partial y}\right)},$$

$$T_{yz} = \frac{C_n}{2}\left(\frac{\partial^2 v_0}{\partial x \partial y} - \frac{\partial^2 u_0}{\partial y^2}\right) + \frac{H_n}{2}\left(\frac{\partial^2 \varphi_y}{\partial x \partial y} - \frac{\partial^2 \varphi_x}{\partial y^2}\right) + \frac{K_{n1}}{2}\varphi_x,$$

$$T_{xz} = \frac{C_n}{2}\left(\frac{\partial^2 v_0}{\partial x^2} - \frac{\partial^2 u_0}{\partial x \partial y}\right) + \frac{H_n}{2}\left(\frac{\partial^2 \varphi_y}{\partial x^2} - \frac{\partial^2 \varphi_x}{\partial x \partial y}\right) - \frac{K_{n1}}{2}\varphi_y,$$

$$L_{xz} = \frac{K_{n1}}{2}\left(\frac{\partial^2 v_0}{\partial x^2} - \frac{\partial^2 u_0}{\partial x \partial y}\right) + \frac{F_n}{2}\left(\frac{\partial^2 \varphi_y}{\partial x^2} - \frac{\partial^2 \varphi_x}{\partial x \partial y}\right) - \frac{K_{n2}}{2}\varphi_y$$

$$L_{yz} = \frac{K_{n1}}{2}\left(\frac{\partial^2 v_0}{\partial x \partial y} - \frac{\partial^2 u_0}{\partial y^2}\right) + \frac{F_n}{2}\left(\frac{\partial^2 \varphi_y}{\partial x \partial y} - \frac{\partial^2 \varphi_x}{\partial y^2}\right) + \frac{K_{n2}}{2}\varphi_x,$$

The constants in Eq. (14) are defined by:

$$(A,B,C,D,F,H)=\int_{-\frac{h}{2}}^{\frac{h}{2}}(1,z,f(z),z^2,zf(z),f(z)^2)\frac{E(z)}{1-\nu^2}dz,$$
$$(A_n,B_n,C_n,D_n,H_n,K_{n1},F_n,K_{n2})=\int_{-\frac{h}{2}}^{\frac{h}{2}}(1,g(z),f(z),g(z)^2,f(z)^2,k(z),k(z)f(z),k(z)^2)\frac{l^2E(z)}{2(1+\nu)}dz \tag{15}$$

By substituting Eq. (14) into Eq. (11), the equilibrium equations on the basis of the displacement field are obtained as follows:

$$\begin{aligned}&A\left(\frac{\partial^2u_0}{\partial x^2}+\frac{1-\nu}{2}\frac{\partial^2u_0}{\partial y^2}+\frac{1+\nu}{2}\frac{\partial^2v_0}{\partial x\partial y}\right)-B\nabla^2\frac{\partial w_0}{\partial x}+C\left(\frac{\partial^2\varphi_x}{\partial x^2}+\frac{1-\nu}{2}\frac{\partial^2\varphi_x}{\partial y^2}+\frac{1+\nu}{2}\frac{\partial^2\varphi_y}{\partial x\partial y}\right)\\&+\frac{A_n}{2}\left(\frac{\partial^4v_0}{\partial x^3\partial y}-\frac{\partial^4u_0}{\partial x^2\partial y^2}+\frac{\partial^4v_0}{\partial x\partial y^3}-\frac{\partial^4u_0}{\partial y^4}\right)\\&+\frac{C_n}{2}\left(\frac{\partial^4\varphi_y}{\partial x^3\partial y}-\frac{\partial^4\varphi_x}{\partial x^2\partial y^2}+\frac{\partial^4\varphi_y}{\partial x\partial y^3}-\frac{\partial^2\varphi_x}{\partial y^4}\right)+\frac{K_{n1}}{2}\left(\frac{\partial^2\varphi_x}{\partial y^2}-\frac{\partial^2\varphi_y}{\partial x\partial y}\right)=0,\end{aligned}$$

$$\begin{aligned}&A\left(\frac{\partial^2v_0}{\partial y^2}+\frac{1-\nu}{2}\frac{\partial^2v_0}{\partial x^2}+\frac{1+\nu}{2}\frac{\partial^2u_0}{\partial x\partial y}\right)-B\nabla^2\frac{\partial w_0}{\partial y}+C\left(\frac{\partial^2\varphi_y}{\partial y^2}+\frac{1-\nu}{2}\frac{\partial^2\varphi_y}{\partial x^2}+\frac{1+\nu}{2}\frac{\partial^2\varphi_x}{\partial x\partial y}\right)\\&+\frac{A_n}{2}\left(-\frac{\partial^4v_0}{\partial x^4}+\frac{\partial^4u_0}{\partial x^3\partial y}-\frac{\partial^4v_0}{\partial x^2\partial y^2}+\frac{\partial^4u_0}{\partial x\partial y^3}\right)\\&+\frac{C_n}{2}\left(-\frac{\partial^2\varphi_y}{\partial x^4}+\frac{\partial^2\varphi_x}{\partial x^3\partial y}-\frac{\partial^2\varphi_y}{\partial x^2\partial y^2}+\frac{\partial^2\varphi_x}{\partial x\partial y^3}\right)+\frac{K_{n1}}{2}\left(-\frac{\partial^2\varphi_x}{\partial x\partial y}+\frac{\partial^2\varphi_y}{\partial x^2}\right)=0,\end{aligned} \tag{16}$$

$$B\nabla^2\left(\frac{\partial u_0}{\partial x}+\frac{\partial v_0}{\partial y}\right)-D\nabla^2w_0+F\nabla^2\left(\frac{\partial\varphi_x}{\partial x}+\frac{\partial\varphi_y}{\partial y}\right)+q_{eff}-A_n\nabla^4w_0+B_n\nabla\left(\frac{\partial\varphi_x}{\partial x}+\frac{\partial\varphi_y}{\partial y}\right)=0,$$

$$\begin{aligned}&C\left(\frac{\partial^2u_0}{\partial x^2}+\frac{1-\nu}{2}\frac{\partial^2u_0}{\partial y^2}+\frac{1+\nu}{2}\frac{\partial^2v_0}{\partial x\partial y}\right)-F\nabla^2\frac{\partial w_0}{\partial x}+H\left(\frac{\partial^2\varphi_x}{\partial x^2}+\frac{1-\nu}{2}\frac{\partial^2\varphi_x}{\partial y^2}+\frac{1+\nu}{2}\frac{\partial^2\varphi_y}{\partial x\partial y}\right)\\&-G(z)A\varphi_x+\frac{1}{2}\left[B_n\left(-\frac{\partial^3w_0}{\partial x\partial y^2}-\frac{\partial^3w_0}{\partial x^3}\right)+\frac{C_n}{2}\left(\frac{\partial^4v_0}{\partial x^3\partial y}-\frac{\partial^4u_0}{\partial x^2\partial y^2}+\frac{\partial^4v_0}{\partial x\partial y^3}-\frac{\partial^4u_0}{\partial y^4}\right)\right.\\&+D_n\left(2\frac{\partial^2\varphi_x}{\partial y^2}-\frac{3}{2}\frac{\partial^2\varphi_y}{\partial x\partial y}+\frac{1}{2}\frac{\partial^2\varphi_x}{\partial x^2}\right)-\frac{K_{n1}}{2}\left(\frac{\partial^2v_0}{\partial x\partial y}-\frac{\partial^2u_0}{\partial y^2}+\frac{\partial^2\varphi_y}{\partial x\partial y}-\frac{\partial^2\varphi_x}{\partial y^2}\right)\\&\left.-\frac{F_n}{2}\left(\frac{\partial^2\varphi_y}{\partial x\partial y}-\frac{\partial^2\varphi_x}{\partial y^2}\right)-\frac{K_{n2}}{2}\varphi_x+\frac{H_n}{2}\left(\frac{\partial^4\varphi_y}{\partial x^3\partial y}-\frac{\partial^4\varphi_x}{\partial x^2\partial y^2}+\frac{\partial^4\varphi_y}{\partial x\partial y^3}-\frac{\partial^4\varphi_x}{\partial y^4}\right)\right]=0,\end{aligned}$$

$$C\left(\frac{\partial^2 v_0}{\partial y^2}+\frac{1-\nu}{2}\frac{\partial^2 v_0}{\partial x^2}+\frac{1+\nu}{2}\frac{\partial^2 u_0}{\partial x\partial y}\right)-F\nabla^2\frac{\partial w_0}{\partial y}+H\left(\frac{\partial^2 \varphi_y}{\partial y^2}+\frac{1-\nu}{2}\frac{\partial^2 \varphi_y}{\partial x^2}+\frac{1+\nu}{2}\frac{\partial^2 \varphi_x}{\partial x\partial y}\right)$$
$$-G(z)A\varphi_y\frac{1}{2}\left[B_n\left(-\frac{\partial^3 w_0}{\partial x^2\partial y}-\frac{\partial^3 w_0}{\partial y^3}\right)+D_n\left(2\frac{\partial^2 \varphi_y}{\partial x^2}-\frac{3}{2}\frac{\partial^2 \varphi_x}{\partial x\partial y}+\frac{1}{2}\frac{\partial^2 \varphi_y}{\partial y^2}\right)\right.$$
$$+\frac{K_{n1}}{2}\left(\frac{\partial^2 v_0}{\partial x^2}-\frac{\partial^2 u_0}{\partial x\partial y}+\frac{\partial^2 \varphi_y}{\partial x^2}-\frac{\partial^2 \varphi_x}{\partial x\partial y}\right)+\frac{F_n}{2}\left(\frac{\partial^2 \varphi_y}{\partial x^2}-\frac{\partial^2 \varphi_x}{\partial x\partial y}\right)-\frac{K_{n2}}{2}\varphi_y$$
$$-\frac{C_n}{2}\left(\frac{\partial^4 v_0}{\partial x^4}-\frac{\partial^4 u_0}{\partial x^3\partial y}+\frac{\partial^4 v_0}{\partial x^2\partial y^2}-\frac{\partial^4 u_0}{\partial x\partial y^3}\right)$$
$$\left.-\frac{H_n}{2}\left(\frac{\partial^4 \varphi_y}{\partial x^4}-\frac{\partial^4 \varphi_x}{\partial x^3\partial y}+\frac{\partial^4 \varphi_y}{\partial x^2\partial y^2}-\frac{\partial^4 \varphi_x}{\partial x\partial y^3}\right)\right]=0$$

The boundary conditions for two cases of simply and clamped supports for all of the edges are presented as the following relations:

- Simply-supported (S):

$$\begin{aligned} &x=0,L_x\ :\ u_0=v_0=w_0=\varphi_y=M_x=0,\\ &y=0,L_y\ :\ u_0=v_0=w_0=\varphi_x=M_y=0 \end{aligned} \tag{17}$$

- Clamped (C):

$$\begin{aligned} &x=0,L_x\ :\ u_0=v_0=w_0=\varphi_y=\varphi_x=0,\\ &y=0,L_y\ :\ u_0=v_0=w_0=\varphi_x=\varphi_y=0 \end{aligned} \tag{18}$$

3. Numerical solution technique

The dynamic relaxation method (DRM) is an iterative process to solve simultaneously the system of equations which its purpose, in general, is transferring a static system to a virtual dynamic one in order to finally obtain a static solution. This technique can be described by mathematics or physics theories. As a mathematical interpretation, this theory is derived according to Richardson's second law. On the other hand, as a physical definition, the DRM can be shown with a steady-state response of a synthesis dynamic system with virtual inertia. It is vivid that the nature of this method is dynamic. Hence, the evaluation steps of the method can be improved with the help of structural dynamic techniques. The repetitive relations of DRM can be obtained by various devices. The finite difference method (FDM) is a very popular one to this end. In addition, a combination of FDM and Newton's second law can be used. Also, the finite element method (FEM) can be contributed to derive DRM formulation. In such a case, from the beginning, the mass and damping forces are entered in the element equations and the element formulation is based on these forces. This technique has been used for analyzing sheet problems. Therefore, the simplest and popular method for iterative techniques can be FDM.

From a mathematical point of view, to increase the speed of the solution, instead of using Newton-Raphson and implicit solution and its difficulties, in fact, the problem is transferred from an implicit one to an explicit one, namely a dynamic problem. Therefore, in the DR method, using this idea, it converts a static problem KX = F to a virtual dynamic problem MA + CV + KX = F, and the problem is basically static but virtually dynamic. Then the dynamic problem is solved and the numerical results will be obtained. There is only one condition for results. It means, those numerical results are correct by which the kinetic energy of the system converges to zero. Our convergence criteria is 10e-12. The iterations will be converged, if the kinetic energy of the system closes to the criteria. Lastly, we convert and transfer a static problem into a virtual dynamic problem and solve it explicitly. Moreover, some methods can be used by which the results can be calculated sooner and

faster, such as Gershgorin theory that makes the Matrices in the diagonal forms and by using such diagonal matrices, the computer code can solve the problem faster.

The static state of governing equations can be written as follows [57]:

$$F(x^{\Delta}) = P \tag{19}$$

in which F is the vector of internal discrete forces, x^{Δ} is the real displacement vector of the discrete system, and P is the vector of external discrete forces. If the real response of Eq. (19), x^{Δ}, is replaced with the approximate response x, the residual force R will be made based on instability of the system:

$$R = P - F(X) \tag{20}$$

A general flowchart associated to the overall procedure of dynamic relaxation technique is outlined below [57-62]

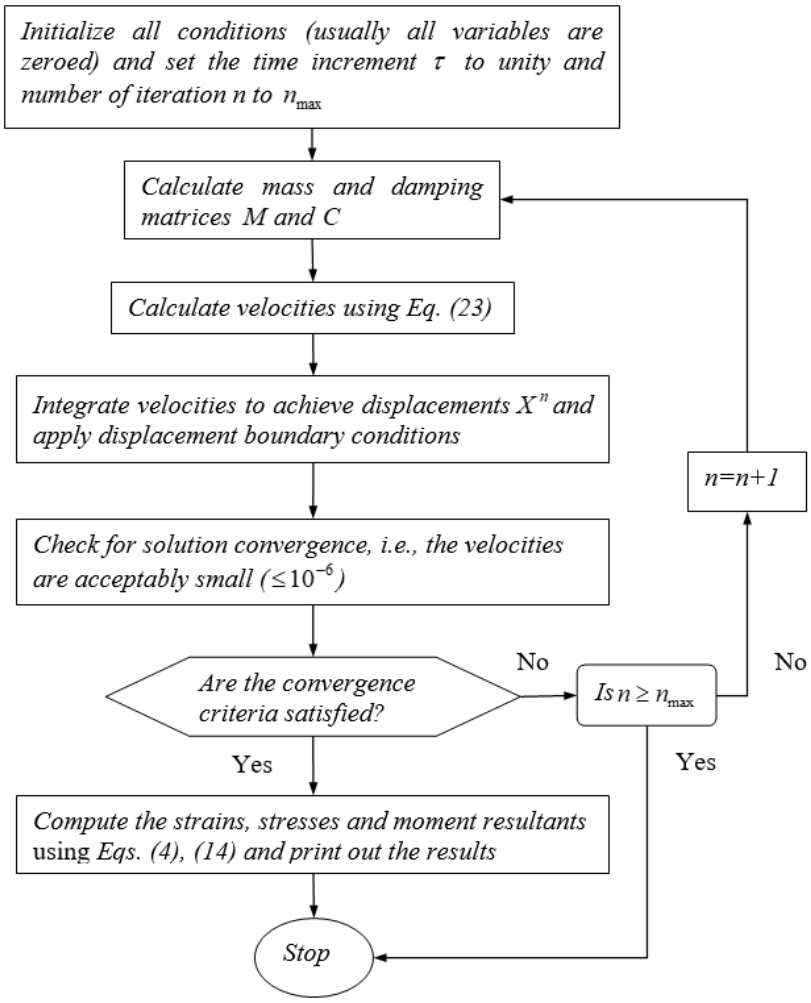

In the DRM, first of all, Eq. (20) is transferred to made dynamical space by adding virtual damping and mass forces.

$$[M]_{DR}^{n}\{a\}^{n} + [C]_{DR}^{n}\{v\}^{n} = \{R\}^{n} \tag{21}$$

in which $[M]_{DR}^{n}$ and $[C]_{DR}^{n}$ are the virtual mass and damping matrices, $\{v\}^{n}$ and $\{a\}^{n}$ are the vectors of speed and acceleration. n also introduces the number of repetitions or steps. Due to the damping of the system, the response of transient state inclines to zero after a specific time, which this time depends on the damping value. Therefore, it can be stated that if a dynamic system is subjected to static load, by spending time the transient response will be zero and the static state solution is

obtained. So, the appropriate selection of virtual damping factors can improve the convergence ratio of the DRM.

By assuming diagonal mass matrix and using central FDM, Eq. (21) can be expressed as follows:

$$R^n = \frac{[M_{DR}]^n}{\tau}\left(\{v\}^{\left(n+\frac{1}{2}\right)} - \{v\}^{\left(n-\frac{1}{2}\right)}\right) + \frac{[C_{DR}]^n}{2}\left(\{v\}^{\left(n+\frac{1}{2}\right)} + \{v\}^{\left(n-\frac{1}{2}\right)}\right) \tag{22}$$

where τ is the time increment.

Eq. (22) can be arranged on the basis of speed in step *n+1/2* and by assuming $[\boldsymbol{C_{DR}}] = \frac{c[\boldsymbol{M}]}{\boldsymbol{\tau}}$ (c is damping constant) in iterative relation, the speed rate in DRM is as follows:

$$\{v\}^{\left(n+\frac{1}{2}\right)} = A\{v\}^{\left(n-\frac{1}{2}\right)} + B\{R\}^n \tag{23}$$

where

$$A = \frac{1-\frac{c}{2}}{1+\frac{c}{2}}, \qquad B = \frac{\tau^n}{2}(1+A)\,[M_{DR}]^{-1} \tag{24}$$

Using Eq. (23) the following iterative equation can be written:

$$\{x\}^{(n+1)} = \{x\}^{(n)} + \tau^{n+1}\{v\}^{\left(n+\frac{1}{2}\right)}, \tag{25}$$

One of the unknown factors in the DRM is the mass matrix. The popular way to obtain the diagonal elements of the mass matrix is the Gerschgorin approach [57]:

$$m_{ii}^i \geq \frac{1}{4}(\tau^n)^2 \sum_{j=1}^{N} |K_{ij}^l|, \tag{26}$$

in which N denotes the degree of freedom of the system and K_{ij}^l is the stiffness matrix defined as follows:

$$[k] = \frac{\partial P}{\partial x} \tag{27}$$

in which P is the left part of the equilibrium equations. This approach, unlike the previous methods, has a strong mathematics logic and the numerical analyses showed that the use of this method reduces the time of calculations. Based on the DRM, a system in the lowest time will converge to a steady response if its damping is equal to the critical value. According to [30], the best way for determining the critical damping is:

$$c^n = 2\left\{\frac{(x^n)^T\, P(x^n)}{(x^n)^T\, M^n\, x^n}\right\}^{\frac{1}{2}}, \tag{28}$$

where x^n is the vector of displacement in step n. In most studies, the time step is constant and the common value is 1 or 1.1. Combining Eq. (19) with Eq. (28) leads to the following dynamic relaxation algorithm:

1. The maximum of iterations, the residual error of internal forces, and strain energy of the structure (e_r, n_{max}, e_k) will be determined.
2. $\{v\}^{-1/2} = 0$, if the kinetic damping is used, the first kinetic energy will be set to zero.
3. $\{x\}^0$, this will be calculated or guessed.
4. The mass matrix is created.
5. If viscous damping is used, the damping matrix is created.
6. The unbalance force ($\{R\}^n$) is calculated.
7. If $|r|_i^n < e_R$, stop; otherwise the calculations will continue.

8. Computing $\{v\}^{n+1/2}$ from Eq. (23).
9. If $\sum_{i=1}^{N} m_{ii}^{n}(v_i^{n+1/2})^2 < e_K$, stop; otherwise the calculations will continue.
10. Computing $\{x\}^{n+1}$ from Eq. (25).
11. Applying the boundary conditions.
12. Substituting $n=n+1$ if $n>n_{max}$, otherwise return to step 4.

The above algorithm shows clearly the advantages of DRM such as simplicity, the vector operator, and also the unique process for both nonlinear and linear systems.

4. Results and discussion

4.1. Convergance rate

In order to consider the mesh sensitivity, in Figure 2 the dimensionless deflection has been illustrated in terms of node numbers (m×n) for x and y axes of the rectangular plate, respectively. As seen from Figure 2, the grid point on the basis of 23 nodes gives acceptable results.

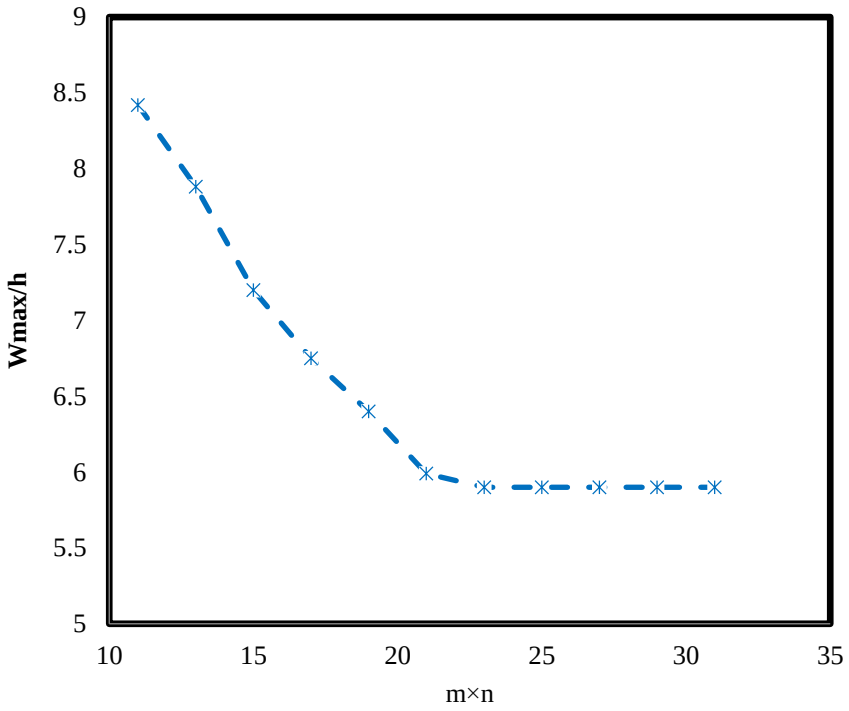

Figure 2. The variation of deflection on the basis of the nodes number.

4.2. Validation of results

To consider the accuracy and precision of the current formulation and results, the bending results of the rectangular nanoplate which are reported by Refs. [63-68] based on different theories and solution methods have been compared with the present responses in Tables 1 to 3 for various loads and boundary conditions. It can be seen from Tables 1 to 3 that the obtained results of this paper are in good agreement with the other reports of Refs. [63-68]. It is noticed that the star sign (*) in Tables 1-3 indicates the nondimensional form of parameters.

Table 1. Comparison of deflection between the current solution and those of Ref. [63, 64] for bending of nanoplate with *($E=25^*$, $L_x^*=L_y^*=100$, $\upsilon=0.3$, $e_0a=0$, $q=0.1^*$).*

B.Cs	h^*	Deflection (w)	
		Present	[63, 64]
CCCC	10	5.163	5.330
CCCC	20	1.053	1.133

Table 2. Comparison of deflection between the current solution and those of Ref. [65] for bending of nanoplate *with (E=1.44 GPa, υ =0.38, q=1 μN/ μm², Lx=500, Ly=500).*

B.Cs	*l* /*h*	Deflection (*w*)	
		Present	[65]
SSSS	1.7	24.37e-5	22.1e-5
SSSS	1	3.65e-4	3.9e-4

Table 3. Comparison of deflection obtained by the current work and those of Ref. [66-68] for (C: L_x^*=100, L_y^*=100, E^*=2.1×10⁶, υ=0.316, q=3*, S: L_x^*=100, L_y^*=100, E^*=2.1×10⁶, υ=0.25, q=1*).

B.Cs	Deflection (*w*)			
	Present	[66]	[67]	[68]
CCCC	1.276	1.123	1.17	1.316
SSSS	1.051	0.944	0.942	1.028

4.3. Aspect ratio effects

Figures 3 and 4 represent the variations of nondimensional deflection of the rectangular nanoplate in terms of aspect ratio and different thickness-to-length ratios for clamped and simply-supported boundary conditions, respectively. As seen, with the increase of aspect ratio, the deflection decreases substantially and the decreasing trend continued till a specific value. It can also be seen that for the aspect ratio of Lx/Ly≥ 2.5, the deflection values converged to a definite value for several thickness-to-length ratios at clamped and simply-supported boundary conditions. In Figures 3 and 4, the value of the uniform transverse load is chosen 5*MPa*, the length of the nanoplate 500 *nm*, and the grading index is selected to 1.

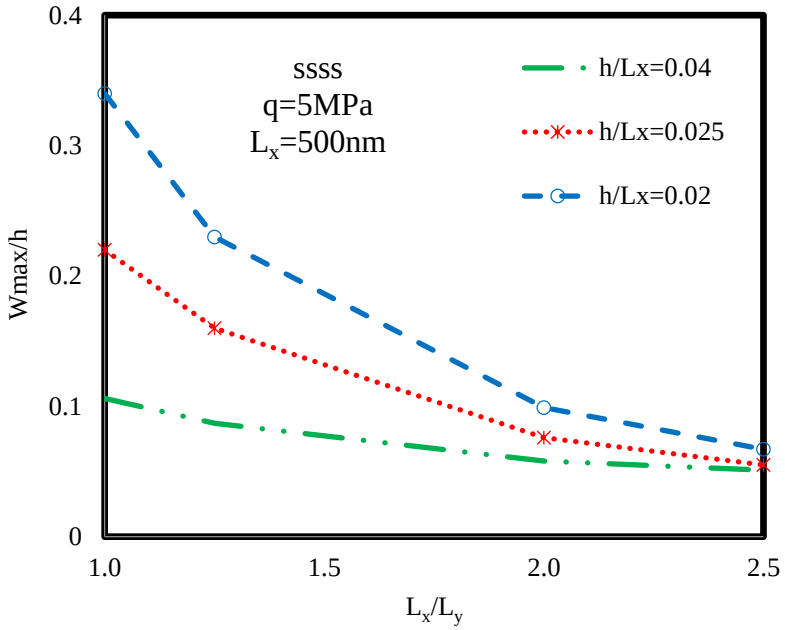

Figure 3. The variations of nondimensional deflection of the rectangular nanoplate in terms of aspect ratio for simply-supported boundary condition and different thickness-to-length ratios.

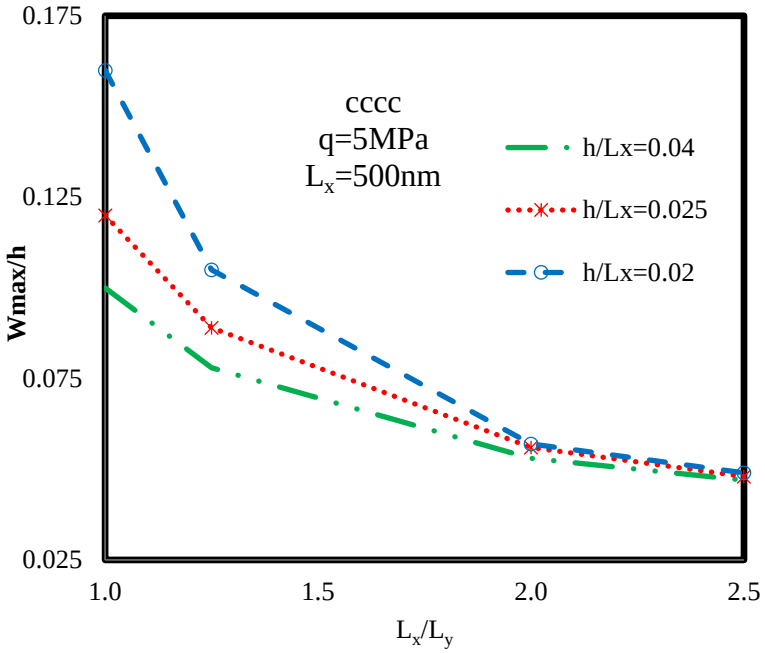

Figure 4. The variations of nondimensional deflection of the rectangular nanoplate in terms of aspect ratio for clamped boundary condition and different thickness-to-length ratios.

Figures 5 and 6 consider the nondimensional deflection of the rectangular nanoplate in terms of aspect ratio and different length scale-to-thickness ratio (*l*/*h*) for simply-supported and clamped boundary conditions, respectively. As shown, with the increase of aspect ratio the deflections go down for different length scale-to-thickness ratios and boundary conditions, and whenever *l*/*h* is greater, this decreasing trend of deflections which originated from the increase of aspect ratios is smaller. Furthermore, whenever *l*/*h* is lower, the deflection of the nanoplate is dramatically affected by a change in dimensions. Also, as indicated in previous figures by increasing the length scale-to-thickness ratio, the deflections decreased and this trend is more significant in simply-supported boundary conditions compared to clamped ones. Similar to previous figures, the grading index is assumed to be 1 in Figures 5 and 6.

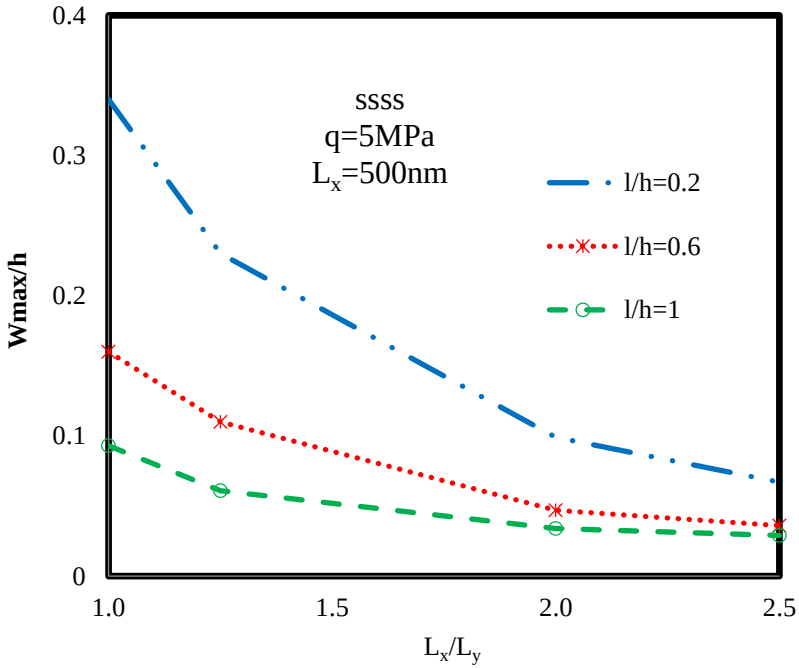

Figure 5. The variations of nondimensional deflection of the rectangular nanoplate based on the aspect ratio and different length scale-to-thickness parameter (l/h) for simple boundary condition.

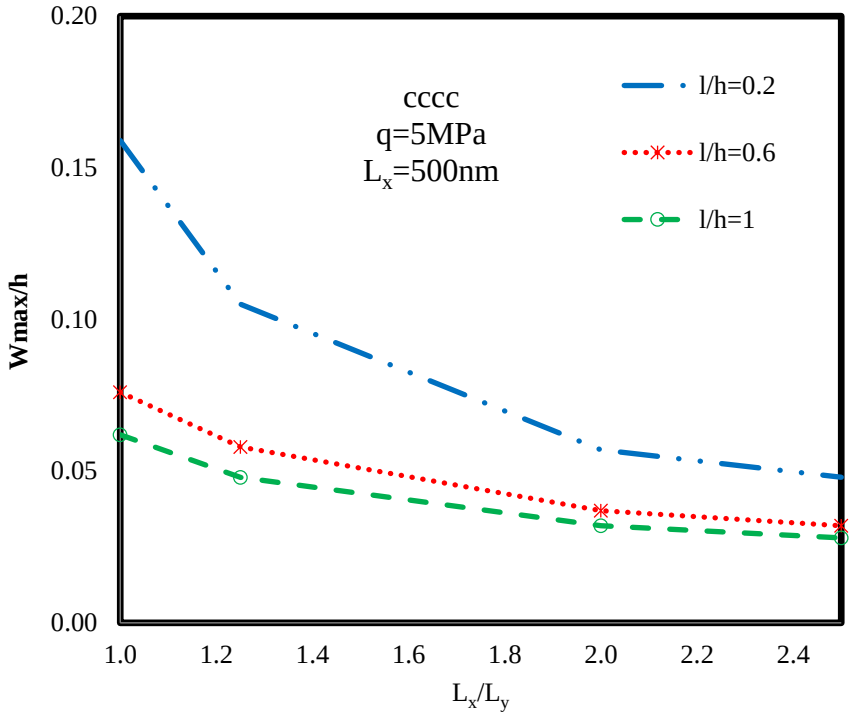

Figure 6. The variations of nondimensional deflection of the rectangular nanoplate based on the aspect ratio and different length scale-to-thickness parameter (l/h) for clamped boundary condition.

Figures 7 and 8 depict the nondimensional deflections of the rectangular nanoplate in terms of aspect ratios and several grading indices for simply-supported and clamped cases, respectively. It can be observed that by varying the aspect ratio the effect of grading index on the results is insignificant for both boundary conditions. As seen, with the increase of aspect ratio, the deflection values decline substantially in clamped boundary condition and similar to clamped cases, rising the aspect ratio causes a decline in deflection for simply-supported cases; however, the rate of this behavior is so slight and falls to a specific value by growing the aspect ratio in simply-supported nanoplates compared to clamped ones. In these diagrams, the length of the nanoplate is 500 nm.

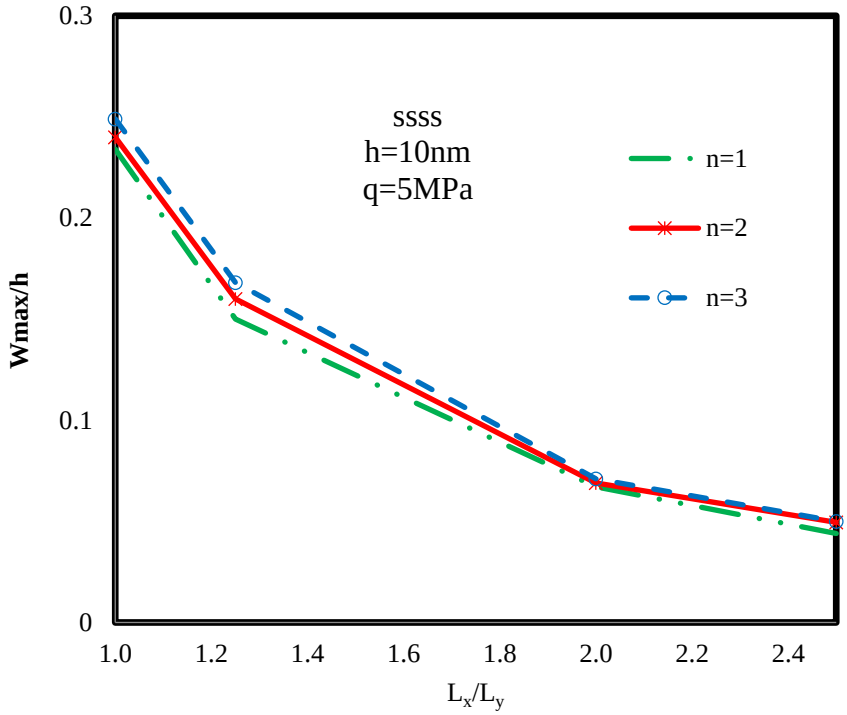

Figure 7. The variations of nondimensional deflection of the rectangular nanoplate based on the aspect ratios and several grading index for simple boundary condition.

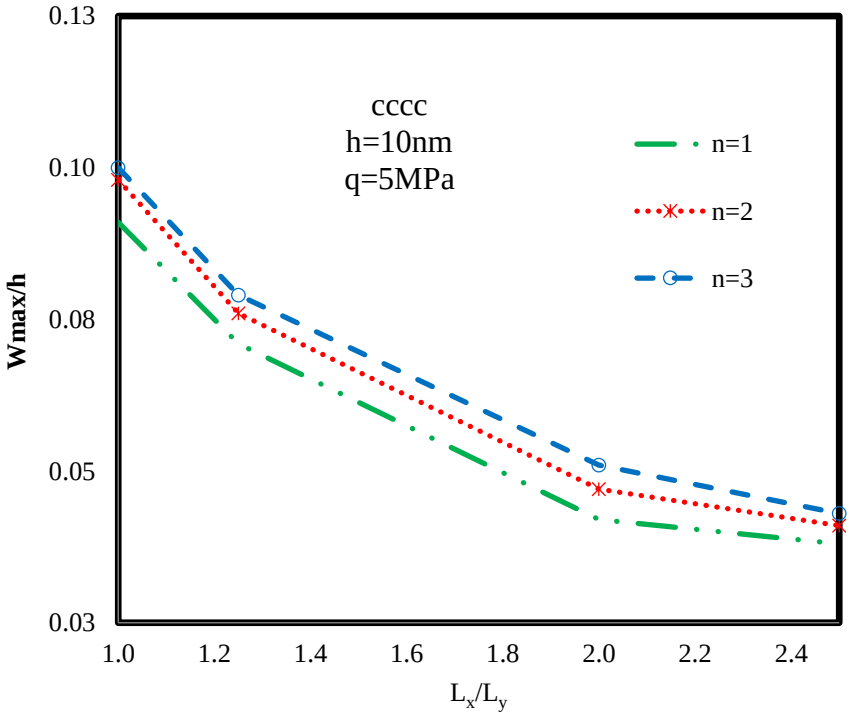

Figure 8. The variations of nondimensional deflection of the rectangular nanoplate based on the aspect ratios and several grading index for clamped boundary condition.

The variations of dimensionless deflection of the rectangular nanoplate are illustrated on the basis of the aspect ratio and different transverse loads in Figures 9 and 10 for simple and clamp boundary conditions, respectively. As seen, the rate of decrease in deflection goes up in greater values of transverse loads. It is observed that at the aspect ratio of 2.5, the deflection curves for various loads tend to a specific value for both clamped and simply-supported boundary conditions. In Figures 9 and 10, the length of the nanoplate is 500 *nm* and the grading index is considered being one.

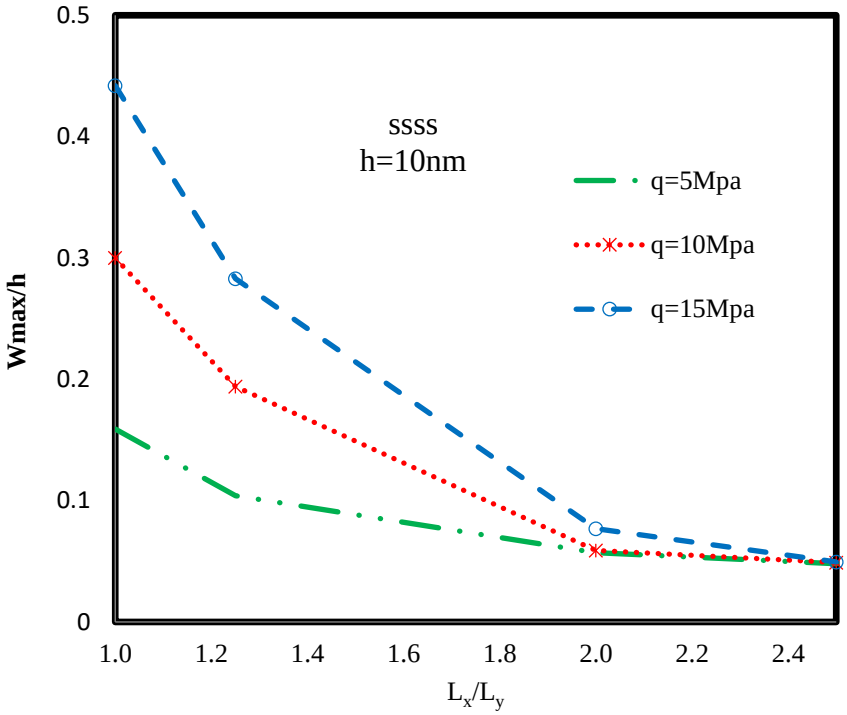

Figure 9. The variations of nondimensional deflection of the rectangular nanoplate in terms of aspect ratios and different transverse loads for simple boundary condition.

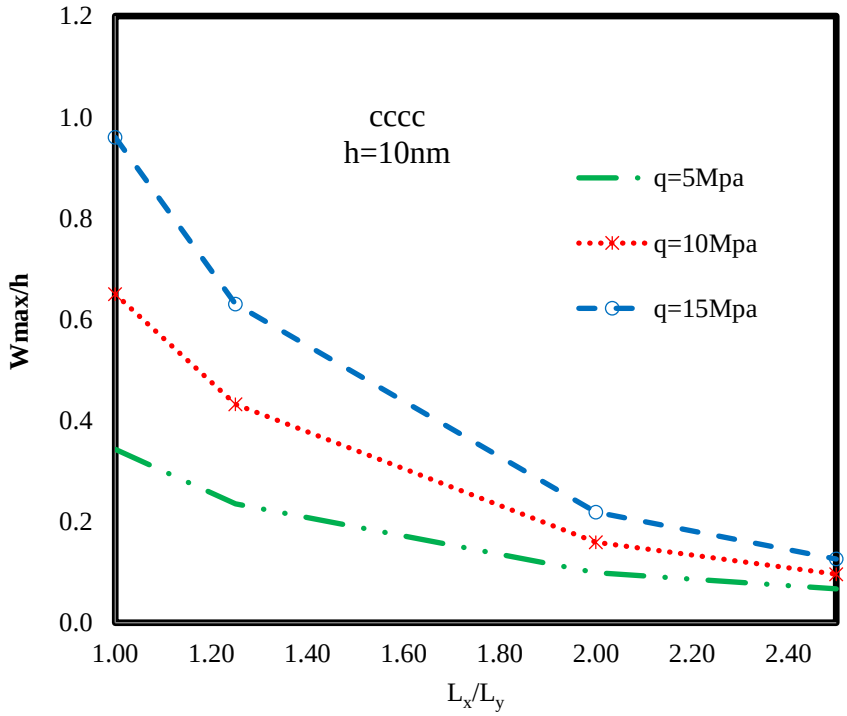

Figure 10. The variations of nondimensional deflection of the rectangular nanoplate in terms of aspect ratios and different transverse loads for clamp boundary condition.

4.4. Grading index effects

Figures 11 and 12 illustrate the dimensionless deflection of the rectangular nanoplate on the basis of the grading index and different length scale-to-thickness ratio (l/h) for clamped and simply-supported boundary conditions, respectively. As seen, with the increase of grading index, the deflection goes up for various ratios of l/h. However, by raising the ratio of l/h the influence of the

grading index on the deflection decreased and by varying the grading index, the deflection remains approximately constant for higher values of *l/h* than 1. Moreover, for lower values of *l/h*, ratio the influence of grading index on the results is much greater in clamped boundary conditions compared to simply one. But, in greater values of this ratio, the variations of deflection are smaller in clamped boundary conditions compared to simply-supported cases. As indicated in Figures 11 and 12, the value of the load is chosen 5*MPa*, the length of the nanoplate is 500 *nm* and the grading index is variable.

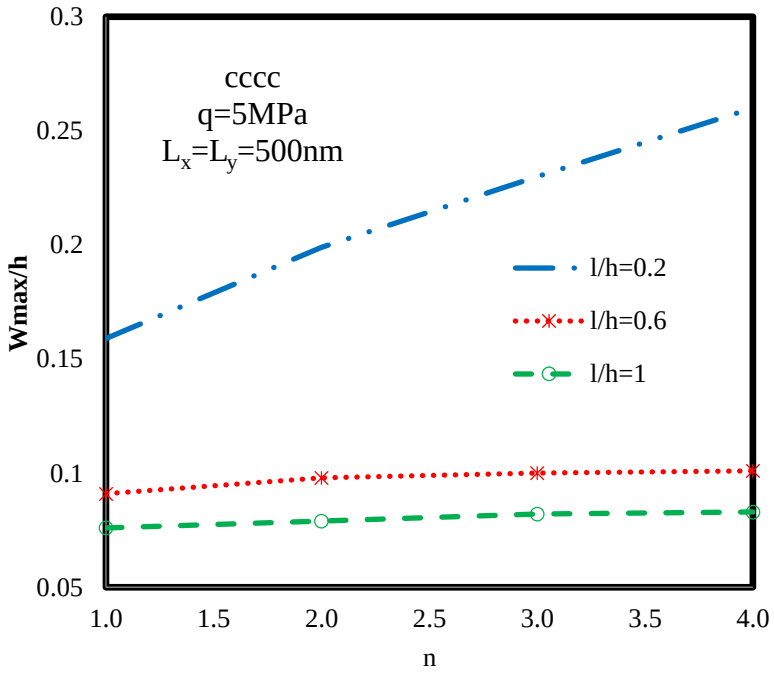

Figure 11. The variations of nondimensional deflection of the rectangular nanoplate in terms of grading index for several length scale-to-thickness ratio and clamped boundary condition.

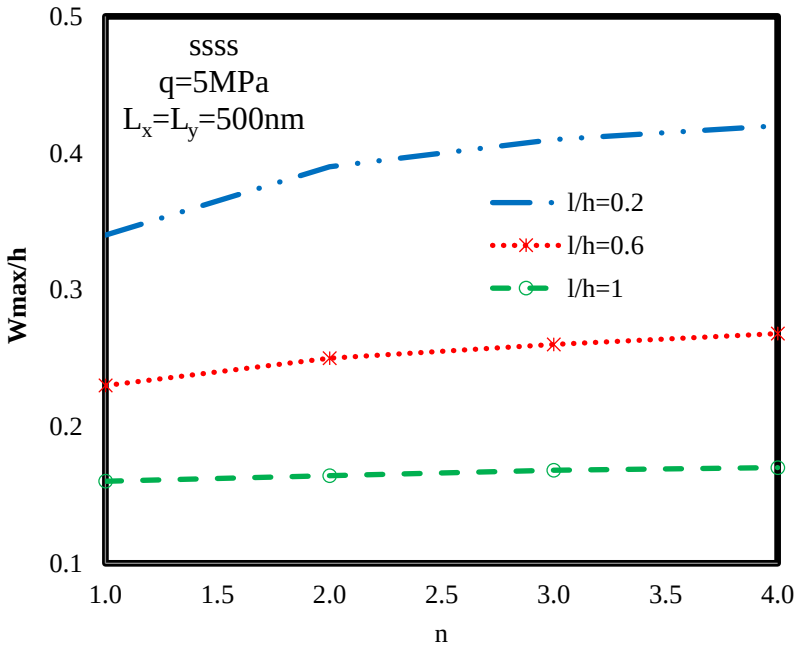

Figure 12. The variations of nondimensional deflection of the rectangular nanoplate in terms of grading index for several length scale-to-thickness ratio and simply-supported boundary condition.

4.5. Length-to-thickness ratio effects

Figures 13 and 14 show the nondimensional deflection of the rectangular nanoplate based on the length scale-to-thickness ratio (l/h) and different thickness-to-length ratio (h/L_x) for clamped and simply-supported boundary conditions, respectively. As shown, whenever h/L_x goes up the deflection of the nanoplate decreases. As observed, varying the thickness-to-length ratios do not have noticeable effects on the deflections in clamped boundary conditions. But, unlike the clamped cases, the thickness-to-length ratio has a significant effect on the results in simply-supported boundary conditions. In addition, by increasing the length scale-to-thickness ratio, the deflections decrease for both cases of clamped and simply-supports. However, the rate of this decrease is much greater in clamped boundary conditions compared to simply-supported ones. Notably, the grading index of the nanoplate has been considered as 1 in Figures 13 and 14.

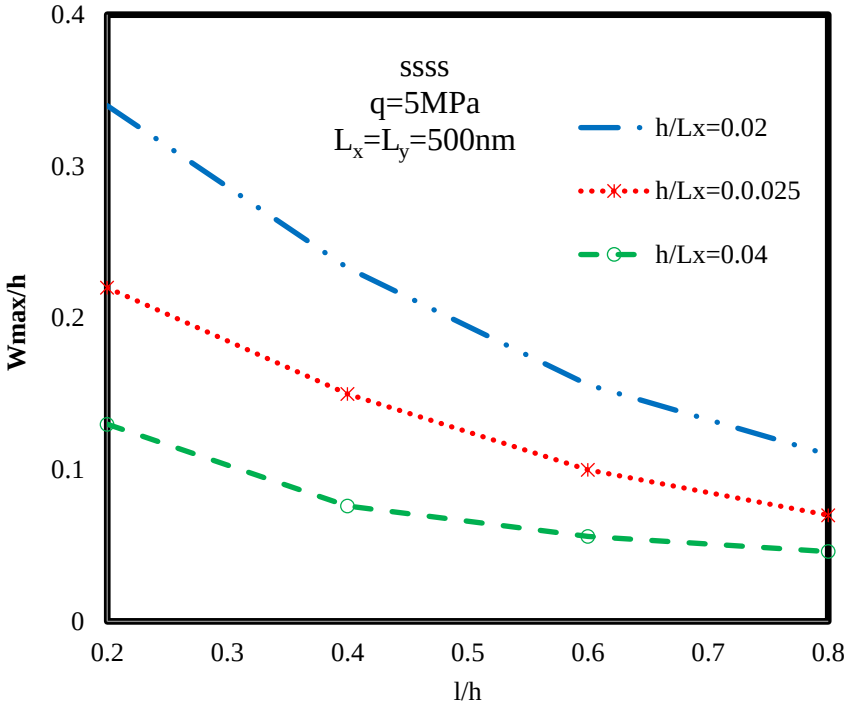

Figure 13. The variations of nondimensional deflection of the rectangular nanoplate based on length scale-to-thickness ratio and different thickness-to-length ratio (h/L_x) for simply-supported boundary condition.

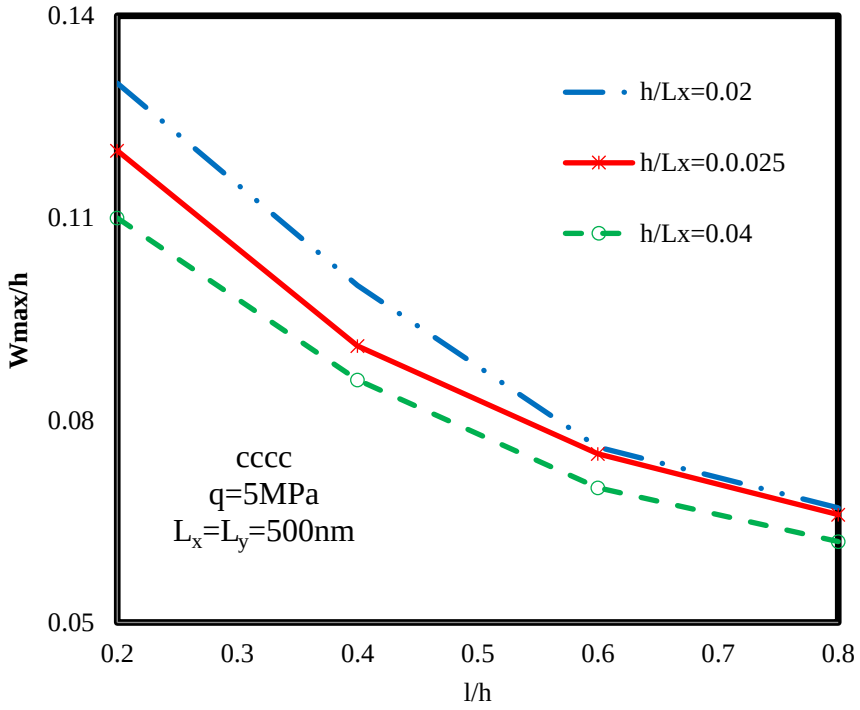

Figure 14. The variations of nondimensional deflection of the rectangular nanoplate based on length scale-to-thickness ratio and different thickness-to-length ratio (h/L_x) for clamped boundary condition.

4.6. Elastic foundation effects

The variations of the dimensionless deflection of the rectangular nanoplate based on the Winkler coefficient and different length scale-to-thickness parameter is shown in Figures 15 and 16 for clamped and simply-supported boundary conditions, respectively. As expected, with increasing the values of Winkler elastic foundation the deflections decreased and by increasing the length scale-to-thickness parameter the decreasing trend is so smoother. These deflections are smaller for the greater l/h and the decreasing trend of them is also smoother. The effect of the elastic foundation on the results is more significant in simply-supported boundary conditions compared to clamp ones. Moreover, it is noticed that with the increase of l/h the influences of elastic foundation decreases. In these diagrams, the value of the grading index is one.

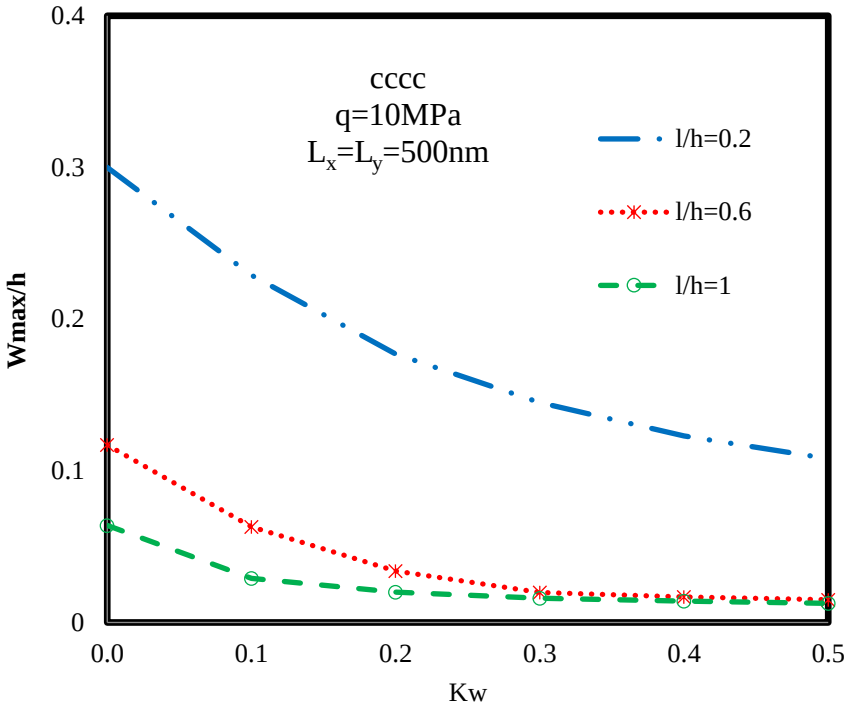

Figure 15. The variations of nondimensional deflection of the rectangular nanoplate based on the Winkler foundation and different length scale-to-thickness parameter for clamped boundary condition.

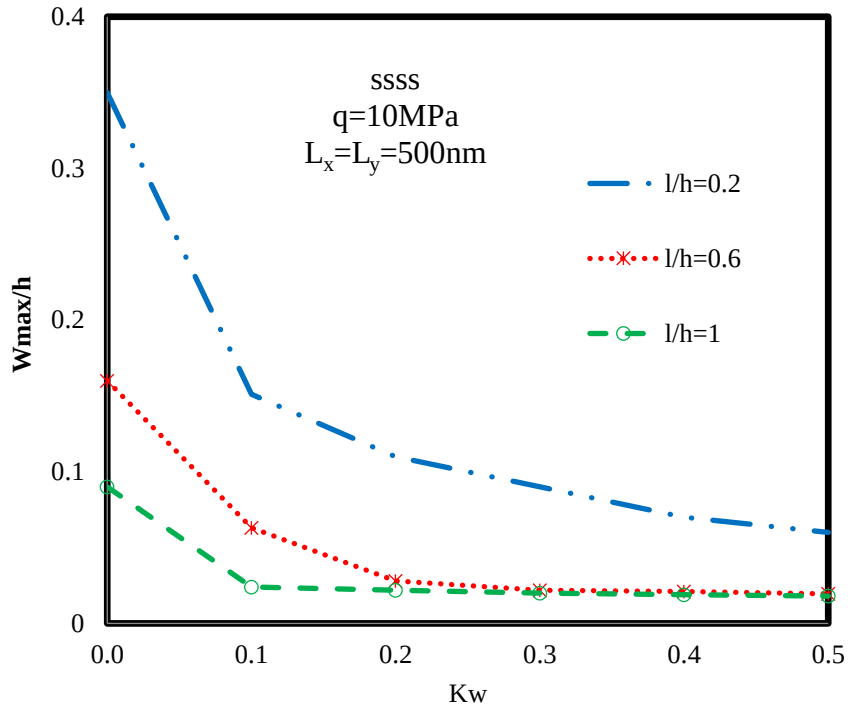

Figure 16. The variations of nondimensional deflection of the rectangular nanoplate based on the Winkler foundation and different length scale-to-thickness parameter for simple boundary condition.

5. Conclusion

In this paper, bending analysis of rectangular functionally graded nanoplates is studied using the modified couple stress theory. The governing equations are derived based on the higher-order shear deformation plate theory. The material properties of nanoplate are assumed to be varying along

the thickness direction according to the simple rule of mixture. In order to solve the equations, the dynamic relaxation method in combination with the finite difference (FD) discretization technique was applied. The deflection of the nanoplate with simply-supported and clamped boundary conditions was investigated for various dimensions, several material grading indexes, different aspect ratios, and elastic foundations. Some significant results are as follows:

- By increasing the length scale-to-thickness ratio, the deflections decreased, and this trend is more significant in simply-supported boundary conditions compared to clamp one.
- By increasing the length scale-to-thickness ratio, the deflections decreased for both cases of clamped and simply-supports. However, the rate of this decrease is much greater in clamped boundary conditions compared to simply-supported ones.
- By rising the length scale-to-thickness ratio the influence of the grading index on the deflection decreased and by varying the grading index, the deflection remains approximately constant for higher values of this ratio than 1.
- For lower values of length scale-to-thickness ratio, the influence of grading index on the results is much greater in clamped boundary conditions compared to simply-supported ones. But, in greater values of this ratio, the variations of deflection are smaller in clamped boundary conditions compared to simply-supported ones.
- Unlike the clamped cases, the thickness-to-length ratio has a significant effect on the results for simply-supported boundary conditions.

Funding: This research received no external funding.

Acknowledgments: V.A.E acknowledges the support of the Government of the Russian Federation (contract No. 14.Z50.31.0046).

Conflicts of Interest: The authors declare no conflict of interest.

References

1. Fleck, N. A.; Muller, G. M.; Ashby, M. F.; Hutchinson, J. W. Strain gradient plasticity: theory and experiment. *Acta Metall Mater* **1994**, 42, 475–487.
2. Stolken, J. S.; Evans, A. G. Microbend test method for measuring the plasticity length scale. *Acta Mater* **1998**, 46, 5109-5115.
3. Fleck, N. A.; Hutchinson, J. W. Phenomenological theory for strain gradient effects in plasticity. *J Mech Phys Solids* **1993**, 41, 1825-1857.
4. Yang, F.; Chong, A. C. M.; Lam, D. C. C.; Tong P. Couple stress based strain gradient theory for elasticity. *Int J Solids Struct* **2002**, 39, 2731-2743.
5. Lam, D. C. C.; Yang, F.; Chong, A. C. M.; Wang, J.; Tong, P. Experiments and theory in strain gradient elasticity. *J Mech Phys Solids* **2003**, 51, 1477-1508.
6. Alibert, J. J.; Seppecher, P.; dell'Isola, F. Truss modular beams with deformation energy depending on higher displacement gradients. *Math Mech Solids* **2003**, 8, 51-73.
7. Giorgio, I. Lattice shells composed of two families of curved Kirchhoff rods: an archetypal example, topology optimization of a cycloidal metamaterial. *Continuum Mech Thermodyn* **2020**. https://doi.org/10.1007/s00161-020-00955-4
8. Giorgio, I.; Ciallella, A.; Scerrato, D. A study about the impact of the topological arrangement of fibers on fiber-reinforced composites: Some guidelines aiming at the development of new ultra-stiff and ultra-soft metamaterials. *Inter J Solids Struct* **2020**, 203, 73-83.
9. De Angelo, M.; Placidi, L.; Nejadsadeghi, N.; Misra, A. Non-standard Timoshenko beam model for chiral metamaterial: Identification of stiffness parameters. *Mech Res Commun* **2020**, 103, 103462.
10. Giorgio, I.; Harrison, P.; dell'Isola, F.; Alsayednoor, J.; Turco, E. Wrinkling in engineering fabrics: a comparison between two different comprehensive modelling approaches. Proceedings of the Royal Society A: Mathematical, Physical and Engineering Sciences **2018**, 474, 20180063.
11. Tsiatas, G. C. New Kirchhoff plate model based on a modified couple stress theory. *Int J Solids Struct* **2009**, 46, 2757–2764.

12. Asghari, M. Geometrically nonlinear micro-plate formulation based on the modified couple stress theory. *Int J Eng Sci* **2012**, 51 292–309.
13. Jomehzadeh, E.; Noori, H. R.; Saidi, A. R. The size-dependent vibration analysis of micro-plates based on a modified couple stress theory. *Physica E* **2011**, 43, 877–883.
14. Akgöz, B.; Civalek, Ö. Modeling and analysis of micro-sized plates resting on elastic medium using the modified couple stress theory. *Meccanica* **2013**, 48, 863–873.
15. Ke, L. L.; Wang, Y. S.; Yang, J.; Kitipornchai, S. Free vibration of size dependent Mindlin micro plates based on the modified couple stress theory. *J Sound Vib* **2012**, 331, 94–106.
16. Roque, C. M. C.; Ferreira, A. J. M.; Reddy, J. N. Analysis of Mindlin micro plates with a modified couple stress theory and a meshless method. *Appl Math Model* **2013**, 37, 4626–4633.
17. Zhang, B.; Liu, Y.; He, D.; Gan, Z.; Shen, L. Non-classical Mindlin plate finite element based on a modified couple stress theory. *Eur. J. Mech. A-Solid* **2013**, 42, 63-80.
18. Ke, L. L.; Yang, J.; Kitipornchai, S.; Bradford, M. A. Bending, buckling and vibration of size-dependent functionally graded annular microplates. *Compos. Struct* **2012**, 94, 3250–3257.
19. Thai, H. T.; Choi, D. H. Size-dependent functionally graded Kirchhoff and Mindlin plate models based on a modified couple stress theory. *Compos Struct* **2013**, 95, 142–153.
20. Thai, H. T.; Kim, S. E. size-dependent functionally graded Reddy plate model based on a modified couple stress theory. *Compos Part B- Eng* **2013**, 45, 1636-1645.
21. Malikan, M. Analytical predictions for the buckling of a nanoplate subjected to nonuniform compression based on the four-variable plate theory. *J Appl Comput Mech* **2017**, 3, 218–228.
22. Malikan, M. Buckling analysis of a micro composite plate with nano coating based on the modified couple stress theory. *J Appl Comput Mech* **2018**, 4, 1–15.
23. Malikan, M. Electro-mechanical shear buckling of piezoelectric nanoplate using modified couple stress theory based on simplified first order shear deformation theory. *Appl Math Model* **2017**, 48, 196–207.
24. Malikan, M. Temperature influences on shear stability of a nanosize plate with piezoelectricity effect. *Multidiscip Model Mater Struct* **2018**, 14, 125–142.
25. Abo-bakr, R. M.; Abo-bakr, H. M.; Mohamed, S. A.; Eltaher, M. A. Optimal weight for buckling of FG beam under variable axial load using Pareto optimality. *Compos Struct* **2021**, 258, 113193.
26. Abdelrahman, A. A.; Abd-El-Mottaleb, H. E.; Eltaher, M. A. On bending analysis of perforated microbeams including the microstructure effects. *Struct Eng Mech* **2020**, 76, 765.
27. Esen, I.; Abdelrahman, A. A.; Eltaher, M. A. Dynamics analysis of Timoshenko perforated microbeams under moving loads. *Eng Comput* **2020**. https://doi.org/10.1007/s00366-020-01212-7
28. Abo-Bakr, R. M.; Eltaher, M. A.; Attia, M. A. Pull-in and freestanding instability of actuated functionally graded nanobeams including surface and stiffening effects. *Eng Comput* **2020**. https://doi.org/10.1007/s00366-020-01146-0
29. Daikh, A. A.; Houari, M. S. A.; Eltaher, M. A. A novel nonlocal strain gradient Quasi-3D bending analysis of sigmoid functionally graded sandwich nanoplates. *Compos Struct* **2020**, 113347. https://doi.org/10.1016/j.compstruct.2020.113347
30. Abdelrahman, A. A.; Mohamed, N. A.; Eltaher, M. A. Static bending of perforated nanobeams including surface energy and microstructure effects. *Eng Comput* **2020**. https://doi.org/10.1007/s00366-020-01149-x
31. Abdelrahman, A. A.; Eltaher, M. A. On bending and buckling responses of perforated nanobeams including surface energy for different beams theories. *Eng Comput* **2020**. https://doi.org/10.1007/s00366-020-01211-8
32. Akgöz, B.; Civalek, Ö. Free vibration analysis of axially functionally graded tapered Bernoulli–Euler microbeams based on the modified couple stress theory. *Compos Struct* **2013**, 98, 314-322.
33. Akgöz, B.; Civalek, Ö. Effects of thermal and shear deformation on vibration response of functionally graded thick composite microbeams. *Compos Part B-Eng* **2017**, 129, 77-87.
34. Dastjerdi, Sh.; Akgöz, B. New static and dynamic analyses of macro and nano FGM plates using exact three-dimensional elasticity in thermal environment. *Compos Struct* **2018**, 192, 626-641.
35. Malikan, M.; Wiczenbach, T.; Eremeyev, V.A. On thermal stability of piezo-flexomagnetic microbeams considering different temperature distributions. *Continuum Mech Thermodyn* **2021**. https://doi.org/10.1007/s00161-021-00971-y
36. Malikan, M. Electro-thermal buckling of elastically supported double-layered piezoelectric nanoplates affected by an external electric voltage. *Multidiscip Model Mater Struct* **2019**, 15, 50-78. https://doi.org/10.1108/MMMS-01-2018-0010

37. Skrzat, A.; Eremeyev, V. A. On the effective properties of foams in the framework of the couple stress theory. *Continuum Mech Thermodyn* **2020**, 32, 1779–1801. https://doi.org/10.1007/s00161-020-00880-6
38. Dastjerdi, Sh.; Malikan, M.; Dimitri, R.; Tornabene, F. Nonlocal elasticity analysis of moderately thick porous functionally graded plates in a hygro-thermal environment. *Compos Struct* **2021**, 255, 112925.
39. Malikan, M.; Eremeyev, V. A. A new hyperbolic-polynomial higher-order elasticity theory for mechanics of thick FGM beams with imperfection in the material composition. *Compos Struct* **2020**, 249, 112486.
40. Malikan, M.; Tornabene, F.; Dimitri, R. Nonlocal three-dimensional theory of elasticity for buckling behavior of functionally graded porous nanoplates using volume integrals. *Mater Res Express* **2018**, 5, 095006.
41. Karami, B.; Shahsavari, D.; Janghorban, M.; Dimitri, R.; Tornabene, F. Wave Propagation of Porous Nanoshells. *Nanomaterials* **2019**, 9, 22.
42. Karami, B.; Janghorban, M.; Shahsavari, D.; Dimitri, R.; Tornabene, F. Nonlocal Buckling Analysis of Composite Curved Beams Reinforced with Functionally Graded Carbon Nanotubes. *Molecules* **2019**, 24, 2750.
43. Ebrahimi-Mamaghani, A.; Forooghi, A.; Sarparast, H.; Alibeigloo, A.; Friswell, M. I. Vibration of viscoelastic axially graded beams with simultaneous axial and spinning motions under an axial load. *Appl Math Modell* **2021**, 90, 131-150.
44. Altenbach, H.; Eremeyev, V.A. On the bending of viscoelastic plates made of polymer foams. *Acta Mech* **2009**, 204, 137.
45. Bîrsan, M.; Altenbach, H.; Sadowski, T.; Eremeyev, V.A.; Pietras, D. Deformation analysis of functionally graded beams by the direct approach. *Compos Part B-Eng* 2012, 43, 1315-1328.
46. Zhang, J.; Zheng, W. Elastoplastic buckling of FGM beams in thermal environment. *Continuum Mech Thermodyn* **2020**. https://doi.org/10.1007/s00161-020-00895-z
47. Roghani, M.; Rouhi, H. Nonlinear stress-driven nonlocal formulation of Timoshenko beams made of FGMs. *Continuum Mech Thermodyn* **2020**. https://doi.org/10.1007/s00161-020-00906-z
48. Yang, F., Chong, A. C. M.; Lam, D. C. C.; Tong, P. Couple stress based strain gradient theory for elasticity. *Int J Solids Struct* **2002**, 39, 2731–274.
49. Soltani, D.; Akbarzadeh Khorshidi, M.; Sedighi, H. M. Higher order and scale-dependent micro-inertia effect on the longitudinal dispersion based on the modified couple stress theory. *J Comput Des Eng*, **2021**, 8, 189-194.
50. Akbarzadeh Khorshidi, M. The material length scale parameter used in couple stress theories is not a material constant. *Inter J Eng Sci* **2018**, 133, 15-25.
51. Nateghi, A.; Salamat-talab, M. Thermal effect on size dependent behavior of functionally graded microbeams based on modified couple stress theory. *Compos Struct* **2013**, 96, 97–110.
52. Lam, D. C. C.; Yang, F.; Chong, A. C. M.; Wang, J.; Tong, P. Experiments and theory in strain gradient elasticity. *J Mech Phy Solids* **2003**, 51, 1477–508.
53. Ke, L-L.; Wang, Y-S. Size effect on dynamic stability of functionally graded microbeams based on a modified couple stress theory. *Compos Struct* **2011**, 93, 342–50.
54. Ma, H. M.; Gao, X. L.; Reddy, J. N. A microstructure-dependent Timoshenko beam model based on a modified couple stress theory. *J Mech Phy Solids* **2008**, 56, 3379–91.
55. Kiarasi, F.; Babaei, M.; Dimitri, R.; Tornabene, F. Hygrothermal modeling of the buckling behavior of sandwich plates with nanocomposite face sheets resting on a Pasternak foundation. *Continuum Mech Thermodyn* **2020**. https://doi.org/10.1007/s00161-020-00929-6
56. Ahmad Pour, M.; Golmakani, M. E; Malikan, M. Thermal Buckling Analysis of Circular Bilayer Graphene Sheets Resting on an Elastic Matrix Based on Nonlocal Continuum Mechanics. *J Appl Comput Mech* **2019**. doi: 10.22055/jacm.2019.31299.1859
57. Zhang, L. C.; Kadkhodayan, M.; Mai, Y. Development of the maDR method. *Comput Struct* **1994**, 52, 1-8.
58. Day, A. S. An introduction to Dynamic Relaxation. *The Engineer* **1965**, 219, 218-221.
59. Salehi, M.; Sobhani, A. R. Elastic linear and non-linear analysis of fiber-reinforced symmetrically laminated sector Mindlin plate. *Compos Struct* **2004**, 65, 65-79.
60. Turvey, G. J.; Salehi, M. Elasto-plastic large deflection response of pressure loaded circular plates stiffened by a single diametral stiffener. *Thin-Walled Struct* **2008**, 46, 991-1002.
61. Kadkhodayan, M.; Golmakani, M. E. Non-linear bending analysis of shear deformable functionally graded rotating disk, *Int J Nonlin Mech* **2014**, 58, 41-56.

62. Golmakani, M. E.; Kadkhodayan, M. Nonlinear bending analysis of annular FGM plates using higher-order shear deformation plate theories. *Compos Struct* **2011**, 93, 973-982.
63. Golmakani, M. E.; Sadraee Far, M. N. Nonlinear thermo-elastic bending behavior of graphene sheets embedded in an elastic medium based on nonlocal elasticity theory. *Comput Math with Appl* **2016**, 72, 785-805.
64. Golmakani, M. E.; Rezatalab, J. Nonlinear bending analysis of orthotropic nanoscale plates in an elastic matrix based on nonlocal continuum mechanics. *Compos Struct* **2014**, 111, 85-97.
65. Akbaş, Ş. D. Static analysis of a nano plate by using generalized differential quadrature method. *Int J Eng Appl Sci* **2016**, 8, 30-39.
66. Chen, W.; Shu, C.; He, W.; Zhong, T. The application of special matrix product to differential quadrature solution of geometrically nonlinear bending of orthotropic rectangular plates. *Comput Struct* **2000**, 74, 65-76.
67. Zhu, G; Wang, H. Quasi-conforming penalty FEM for large deflection of composite laminated plate. *Acta Mater Compos Sinica* **1989**, 6, 39-47.
68. Bazeley, G. P.; Cheung, Y. K.; Irens, B. M.; Zienkiewicz, O. C. Triangular elements in bending-conforming and non-conforming solutions. In: Przemieniecki JS, et al., editors. Proceedings of Conference on Matrix Methods in Structural Mechanics, OH, Wright-Patterson Air Force Base: Air Force Institute of Technology **1965**, 547±76.